Non-thermal desorption/ablation of molecular solids induced by ultra-short soft x-ray pulses

J. Chalupský[1,2,*], L. Juha[1], V. Hájková[1], J. Cihelka[1], L. Vyšín[1,2], J. Gautier[3], J. Hajdu[6], S. P. Hau-Riege[7], M. Jurek[5], J. Krzywinski[5], R. A. London[7], E. Papalazarou[3], J. B. Pelka[5], G. Rey[3], S. Sebban[3], R. Sobierajski[5], N. Stojanovic[4], K. Tiedtke[4], S. Toleikis[4], T. Tschentscher[4], C. Valentin[3], H. Wabnitz[4], and P. Zeitoun[3]

[1]*Institute of Physics, Academy of Sciences of the Czech Republic, Na Slovance 2, 182 21 Prague 8, Czech Republic*
[2]*Czech Technical University in Prague, Zikova 4, 166 36 Praha 1, Czech Republic*
[3]*Laboratoire d'Optique Appliquée, École Polytechnique, ENSTA, CNRS, F-91761 Palaiseau, France*
[4]*Deutsches Elektronen-Synchrotron DESY, Notkestrasse 85, D-22603 Hamburg, Germany*
[5]*Institute of Physics, Polish Academy of Sciences, Al. Lotników 32/46, PL-02-668 Warsaw, Poland*
[6]*Biomedical Centre, Uppsala University, Uppsala, SE-75124 Sweden*
[7]*Lawrence Livermore National Laboratory, 7000 East Avenue, Livermore, CA 94550, USA*

*chal@fzu.cz

http://www.fzu.cz; http://www.cvut.cz

Abstract: We report the first observation of single-shot soft x-ray laser induced desorption occurring below the ablation threshold in a thin layer of poly (methyl methacrylate) - PMMA. Irradiated by the focused beam from the Free-electron LASer in Hamburg (FLASH) at 21.7nm, the samples have been investigated by atomic-force microscope (AFM) enabling the visualization of mild surface modifications caused by the desorption. A model describing non-thermal desorption and ablation has been developed and used to analyze single-shot imprints in PMMA. An intermediate regime of materials removal has been found, confirming model predictions. We also report below-threshold multiple-shot desorption of PMMA induced by high-order harmonics (HOH) at 32nm. Short-time exposure imprints provide sufficient information about transverse beam profile in HOH's tight focus whereas long-time exposed PMMA exhibits radiation-initiated surface hardening making the beam profile measurement infeasible.

OCIS codes: (140.7240) Lasers and laser optics: UV, XUV, and X-ray lasers; (140.2600) Lasers and laser optics: Free electron lasers; (140.3330) Laser damage.

References and links

1. V. Ayvazyan et. al., "A new powerful source for coherent VUV radiation: Demonstration of exponential growth and saturation at the TTF free-electron laser," Eur. Phys. J. **D20**, 149–156 (2002).
2. V. Ayvazyan et. al., "Generation of GW radiation pulses from a VUV free-electron laser operating in the femtosecond regime," Phys. Rev. Lett. **88**, 104802 (2002).
3. V. Ayvazyan et. al., "First operation of a free-electron laser generating GW power radiation at 32 nm wavelength," Eur. J. Phys. **D37**, 297-303 (2006).
4. B. Rus, T. Mocek, A. R. Präg, M. Kozlová, G. Jamelot, A. Carillon, D. Ros, D. Joyeux, and D. Phalippou, "Multi-millijoule, highly coherent X-ray laser at 21 nm operating in deep saturation through double-pass amplification," Phys. Rev. **A66**, 063806-12 (2002).
5. B. Rus, A. Carillon, P. Dhez, P. Jaeglé, G. Jamelot, A. Klisnick, M. Nantel, and P. Zeitoun, "An efficient, high-brightness soft X-ray laser at 21.2 nm," Phys. Rev. **A55**, 3858–3873 (1997).
6. P. Balcou, R. Haroutunian, S. Sebban, G. Grillon, A. Rousse, G. Mullot, J. P. Chambaret, G. Rey, A. Antonetti, D. Hulin, L. Roos, D. Descamps, M. B. Gaarde, A. L'Huillier, E. Constant, E. Mevel, D. von der Linde, A. Orisch, A. Tarasevitch, U. Teubner , D. Klopfel, and W. Theobald, "High-order-harmonic generation: towards laser-induced phase-matching control and relativistic effects," Appl. Phys. **74**, 509-515 (2002).

7. S. Kazamias, D. Douillet, F.Weihe, C. Valentin, A. Rousse, S. Sebban, G. Grillon, F. Auge´, D. Hulin, and Ph. Balcou, "Global optimization of high harmonic generation," Phys. Rev. Lett. **90**, 193901 (2003).
8. J. J. Rocca, V. N. Shlyaptsev, F. G. Tomasel, O. D. Cortazar, D. Hartshorn, and J. L. A. Chilla, "Demonstration of a discharge pumped table-top soft-X-ray laser," Phys. Rev. Lett. **73**, 2192-2195 (1994).
9. S. Heinbuch, M. Grisham, D. Martz, and J. J. Rocca, "Demonstration of a desk-top size high repetition rate soft x-ray laser," Opt. Express **13,** 4050-4055 (2005).
10. P. E. Dyer, "Excimer laser polymer ablation: twenty years on," Appl. Phys. **A77**, 167-173 (2003), and references cited therein.
11. L. V. Zhigilei, B. J. Garrison, "Molecular dynamics simulation study of the fluence dependence of particle yield and plume composition in laser desorption and ablation of organic solids," Appl. Phys. Lett. **74,** 1341-1343 (1999).
12. J. Krzywinski, R Sobierajski, M. Jurek, R. Nietubyc, J. B. Pelka, L. Juha, M. Bittner, V. Létal, V. Vorlíček, A. Andrejczuk, J. Feldhaus, B. Keitel, E. L. Saldin, E. A. Schneidmiller, R. Treusch, M. V. Yurkov, "Conductors, semiconductors, and insulators irradiated with short-wavelength free-electron laser," J. Appl. Phys. **101**, 043107 (2007).
13. L. Juha, J. Krása, A. Präg, A. Cejnarová, D. Chvostová, K. Rohlena, K. Jungwirth, J. Kravárik, P. Kubeš, Yu. L. Bakshaev, A. S. Chernenko, V. D. Korolev, V. I. Tumanov, M. I. Ivanov, A. Bernardinello, J. Ullschmied, F. P. Boody, "Ablation of poly(methyl methacrylate) by a single pulse of soft X-rays emitted from Z-pinch and laser-produced plasmas," Surf. Rev. Lett. **9**, 347-352 (2002).
14. L. Juha, M. Bittner, D. Chvostová, J. Krása, Z. Otcenasek, A. R. Präg, J. Ullschmied, Z. Pientka, J. Krzywinski, J. B. Pelka, A. Wawro, M. E. Grisham, G. Vaschenko, C. S. Menoni, and J. J. Rocca, "Ablation of organic polymers by 46.9-nm laser radiation," Appl. Phys. Lett. **86**, 034109 (2005).
15. L. Juha, M. Bittner, D. Chvostová, J. Krása, M. Kozlová, M. Pfeifer, J. Polan, A. R. Präg, B. Rus, M.Stupka, J. Feldhaus, V. Létal, Z. Otcenasek, J. Krzywinski, R. Nietubyc, J. B. Pelka, A. Andrejczuk, R. Sobierajski, L. Ryc, F. P. Boody, H. Fiedorowicz, A. Bartnik, J. Mikolajczyk, R. Rakowski, P. Kubat, L. Pína, M. Horvath, M. E. Grisham, G. O. Vaschenko, C. S. Menoni, J. J. Rocca, "Short-wavelength ablation of molecular solids: pulse duration and wavelength effects," J. Microlith. Microfab. Microsyst. **4**, 033007 (2005), and references cited therein.
16. J. Chalupsky, L. Juha, J. Kuba, J. Cihelka, V. Hájková, M. Bergh, R. M. Bionta, C. Caleman, H. Chapman, J. Hajdu, S. P. Hau-Riege, M. Jurek, S. Koptyaev, J. Krása, A. Krenz-Tronnier, J. Krzywinski, R. A. London, J. Meyer-ter-Vehn, R. Nietubyc, J. B. Pelka, R. Sobierajski, K. Sokolowski-Tinten, N. Stojanovic, K. Tiedtke, S. Toleikis, T. Tschentscher, A. Velyhan, H. Wabnitz, U. Zastrau, "Ablation of organic molecular solids by focused soft X-ray free-electron laser radiation," in Proceedings of the 10th International Conference on X-ray Lasers – ICXRL 2006, P. V. Nickles, K. A. Janulewicz, ed. (Springer-Verlag, 2007), pp. 503-510.
17. J. Chalupský, L. Juha, J. Kuba, V. Hájková, J. Cihelka, P. Homer, M. Kozlová, T. Mocek, J. Polan, B. Rus, J. Krzywinsky, R. Sobierajski, H. Wabnitz, J. Feldhaus, K. Tiedtke, "Utilizing ablation of solids to characterize a focused soft x-ray laser beam," Proc. SPIE **6586**, 65860S-1 (2007).
18. S. P. Hau-Riege, R. A. London, R. M. Bionta, M. A. McKernan, S. L. Baker, J. Krzywinski, R. Sobierajski, R. Nietubyc, J. B. Pelka, M. Jurek, L. Juha, J. Chalupsky, J. Cihelka, V. Hajkova, A. Velyhan, J. Krasa, J. Kuba, K. Tiedtke, S. Toleikis, T. Tschentscher, H. Wabnitz, M. Bergh, C. Caleman, K. Sokolowski-Tinten, N. Stojanovic, U. Zastrau, "Damage threshold of inorganic solids under free-electron-laser irradiation at 32.5 nm wavelength," Appl. Phys. Lett. **90**, 173128 (2007).
19. N. Stojanovic, D. von der Linde, K. Sokolowski-Tinten, U. Zastrau, F. Perner, E. Foerster, R. Sobierajski, R. Nietubyc, M. Jurek, D. Klinger, J. Pelka, J. Krzywinski, L. Juha, J. Cihelka, A. Velyhan, S. Koptyaev, V. Hajkova, J. Chalupsky, J. Kuba, T. Tschentscher, S. Toleikis, S. Duesterer, H. Redlin, "Ablation of solids using a femtosecond extreme ultraviolet free electron laser," Appl. Phys. Lett. **89**, 241909 (2006).
20. R. F. Haglund, "Microscopic and mesoscopic aspects of laser-induced desorption and ablation," Appl. Surf. Sci. **96-98**, 1-13 (1996).
21. J. M. Liu, "Simple technique for measurements of pulsed Gaussian-beam spot sizes", Opt. Lett. **7**, 196-198 (1982).
22. J. Chalupský, L. Juha, J. Kuba, J. Cihelka, V. Hájková, S. Koptyaev, J. Krása, A. Velyhan, M. Bergh, C. Caleman, J. Hajdu, R. M. Bionta, H. Chapman, S. P. Hau-Riege, R. A. London, M. Jurek, J. Krzywinski, R. Nietubyc, J. B. Pelka, R. Sobierajski, J. Meyer-ter-Vehn, A. Tronnier, K. Sokolowski-Tinten, N. Stojanovic, K. Tiedtke, S. Toleikis, T. Tschentscher, H. Wabnitz, U. Zastrau, "Characteristics of focused soft X-ray free-electron laser beam determined by ablation of organic molecular solids," Opt. Express **15**, 6036 (2007).
23. M. Richter, A. Gottwald, U. Kroth, A.A. Sorokin, S. V. Bobashev, L. A. Shmaenok, J. Feldhaus, C. Gerth, B. Steeg, K. Tiedtke, R. Treusch, "Measurement of gigawatt radiation pulses from a vacuum and extreme ultraviolet free-electron laser," Appl. Phys. Lett **83**, 2970-2972 (2003).
24. S. Düsterer, P. Radcliffe, G. Geloni, U. Jastrow, M. Kuhlmann, E. Plönjes, K. Tiedtke, R. Treusch, J. Feldhaus, P. Nicolosi, L. Poletto, P. Yeates, H. Luna, J. T. Costello, P. Orr, D. Cubaynes and M. Meyer, "Spectroscopic characterization of vacuum ultraviolet free electron laser pulses," Opt. Lett. **31**, 1750-1752 (2006).

25. L. V. Zhigilei, Y. G. Yingling, T. E. Itina, T. A. Schoolcraft, B. J. Garrison, "Molecular dynamics simulations of matrix-assisted laser desorption - connections to experiment," Int. J. Mass Spectr. **226**, 85–106 (2003).
26. I. Horcas, R. Fernandez, J. M. Gomez-Rodriguez, J. Colchero, J. Gomez-Herrero, A. M. Baro, "WSXM: A software for scanning probe microscopy and a tool for nanotechnology," Rev. Sci. Instrum. **78**, 013705 (2007).
27. D. A. G. Deacon, "Optical coating damage and performance requirements in free electron lasers," Nucl. Instrum. Meth. Phys. Res. **A250**, 283-288 (1986).
28. E. M. Lehockey, I. Reid and I. Hill, "The radiation chemistry of poly(methyl methacrylate) polymer resists", J. Vac. Sci. Technol. **A6**, 828-832 (1997).
29. T. Mocek, B. Rus, M. Kozlová, M. Stupka, A. R. Präg, J. Polan, M. Bittner, R. Sobierajski and L. Juha, "Focusing a multimillijoule soft x-ray laser at 21 nm," Appl. Phys. Lett. **89**, 051501 (2006).
30. M. De Grazia, H. Merdji, B. Carré, J. Gaudin, G. Geoffroy, S. Guizard, N. Fedorov, A. Belsky, P. Martin, M. Kirm, V. Babin, E. Feldbach, S. Vielhauer, V. Nagirnyi, A. Vassil'ev, F. Krejci, J. Kuba, J. Chalupsky, J. Cihelka, V. Hajkova, M. Ledinský, L. Juha, "Applications of intense ultra-short XUV pulses to solid state physics: time-resolved luminescence spectroscopy and radiation damage studies," Proc. SPIE **6586**, 65860I-1 (2007).
31. F. Barkusky, C. Peth, A. Bayer, K. Mann, "Direct photo-etching of poly(methyl methacrylate) using focused extreme ultraviolet radiation from a table-top laser-induced plasma source," J. Appl. Phys. **101**, 124908 (2008).
32. C. Peth, F. Barkusky, K. Mann, "Near-edge x-ray absorption fine structure measurements using a laboratory-scale XUV source," J. Phys. **D41**, 105202 (2008).

1. Introduction

In the last decades, rapid development of soft x-ray and XUV lasers opened a relatively new area of the laser-matter interaction. These sources represented, for example, by free-electron lasers [1-3], laser-produced plasma-based lasers [4,5], high-order harmonics [6,7], and capillary discharge lasers [8,9], provide a large variety of interaction conditions. In the soft x-ray and XUV spectral domains, laser-matter interaction processes are strongly influenced by laser parameters, i.e., pulse energy, pulse duration, central wavelength, peak intensity, etc. Therefore, intense investigation and modeling of such exotic interactions are needed. Detailed description of soft x-ray laser-matter interaction is of high importance for various scientific disciplines and applications such as photolithography, optical components development, and radiation chemistry.

Our field of interest in the area of soft x-ray laser-matter interactions is damage to various solids. During the last several decades, both laser-induced ablation and desorption were extensively studied in IR-vis-UV spectral ranges [10,11]. Therefore, these are relatively well-understood phenomena at longer wavelengths. An extension of ablation studies into soft x-ray/XUV region has been enabled by the above-mentioned development of new sources. A few papers have been published dealing with topics of soft x-ray/XUV laser damage to various solid materials [12-19,22], primarily motivated by testing materials for short wavelength optical elements. All of the reflecting optical components used in soft x-ray beamlines have to be resistant to damage by energetic photons (30eV – 200eV), but also have to provide the highest possible reflectivity for a long period of time. Therefore, the investigation of material damage mechanisms is crucial for the development and use of such soft x-ray optical devices.

Until recently, material ablation was the main aim of our studies. However, there is another effect responsible for material removal, known in laser and synchrotron radiation communities as material desorption and direct (vacuum) photo-etching, respectively. The processes of desorption and ablation were systematically studied and distinguished by Haglund [20] in the ultra-violet spectral range. Haglund's criterion defines laser-induced desorption and ablation as less than and more than half of a surface monolayer removed by a single laser pulse, respectively. Thus ablation is characteristically a volume effect occurring at high intensity while desorption is a surface effect at low intensity. Surprisingly, for photons in the soft x-ray spectral domain Haglund's criterion has to be modified. In addition to material

removal, material damage must be associated with changes of optical properties related to structural and chemical surface alteration.

2. Single-shot damage experiments

Our previous XUV/x-ray interaction studies were mainly focused on basic characteristics of single-shot ablation processes, namely the determination of the attenuation length and the ablation threshold [12-19,22]. All of the results were for various solid state materials determined using a method reported by Liu [21] based on the morphology of the ablated crater. From maximal crater depth and damaged area, we were able to evaluate both the material and beam parameters. One important result has been the determination of the transverse profile of the focused FLASH beam from AFM measurements of the crater shape in PMMA [22].

The low intensity process of single-shot desorption has been rarely visible by our microscopy techniques and was not taken into account in our previous analysis. Typically, the soft x-ray laser-induced desorption creates craters several nm in depth and is much weaker than the ablation occurring in depths comparable to the attenuation length. Therefore, the weak desorption imprint of beam's tail is often being overlapped by the deep and wide ablated crater located in the center of interaction area.

To investigate, compare, and distinguish between laser-induced desorption and ablation, we have used two different soft x-ray sources (Tab. 1). These sources have been chosen to provide separated single pulses of comparable durations and wavelengths to match the same laser-matter interaction scheme. On the other hand, essentially differing peak fluence of tightly focused beams provided by the two sources allows the investigation of a broad range of interaction in the intensity, fluence, and dose scale.

Table 1. – Parameters for irradiation experiments.

	FLASH[(a)]	HOH[(b)]
Wavelength	32nm – 7nm	32nm
Avg. pulse energy	10μJ	<10pJ
Pulse duration	20fs	10fs
Focus diameter	20μm	2μm
Avg. peak fluence (in focus)	3J/cm^2	<0.3mJ/cm^2
Avg. peak intensity (in focus)	100TW/cm^2	<20GW/cm^2
Repetition rate:	5Hz	1kHz

[(a)]Free-electron LASer in Hamburg, HASYLAB-DESY/Hamburg – Germany
[(b)]High-order harmonics in Salle Orange, LOA-ENSTA/Palaiseau – France

2.1 Single-shot PMMA damage experiments at FLASH

Damage experiments to various materials (PMMA, amorphous carbon, monocrystalline and amorphous silicon, boron carbide, fused silica, etc.) were conducted at the FLASH facility in September 2006. The laser source parameters are summarized in Tab. 1. FLASH belongs to the new family of tunable short-wavelength lasers providing ultra-short pulses with excellent peak brightness. The operation of FLASH and process of ultra-intense soft x-ray radiation generation in this nearly 300m long laser system is described in [1-3].

Exiting the undulator, the laser beam propagates along an ultra-high vacuum (UHV) beamline involving several diagnostic devices such as pulse energy measuring gas monitor detector (GMD) [23], a variable line spacing grating spectrometer (VLS) [24], optional ionizing gas monitor measuring the beam profile, etc. A gas attenuator is used to vary the average pulse energy and a pair of selectable circular apertures allows the suppression of beam pointing instability and reduces imperfections of the beam profile in the far field. Finally, focused by an elliptical grazing incidence carbon coated mirror with a focal length of 200cm, the beam enters an UHV spherical chamber equipped with translation-rotational target manipulator.

The peak fluence in the tight focus is several J/cm^2 and well exceeds the ablation threshold of PMMA, estimated to be ~10mJ/cm^2 for 21.7nm. The attenuation length at this wavelength was determined to be ~70nm [17]. Accordingly to previously reported beam profile measurements [22], we assume a Gaussian beam profile. Once the peak fluence is greater than the threshold value, the beam maximum appears in the ablation regime whereas beam tails occur in the desorption regime (see Fig. 3 below for a better understanding). Figure 1(a) shows a typical crater created by an attenuated 21.7-nm FLASH pulse (~30mJ/cm^2, normal incidence) in 500-nm thin layer of PMMA (Silson, UK). The blue area in Fig. 1(a), surrounding the main crater, is related to the desorption regime and is well distinguishable from the ablated area in the center. In Fig. 1(b) the transverse cross-section is fitted by function (4) derived below assuming a Gaussian beam profile and neglecting the intermediate regime. Moreover, under the assumption of the Gaussian beam profile, the efficiency curve $\eta(\varepsilon)$ can be obtained from the crater morphology measurement as introduced in Fig. 3.

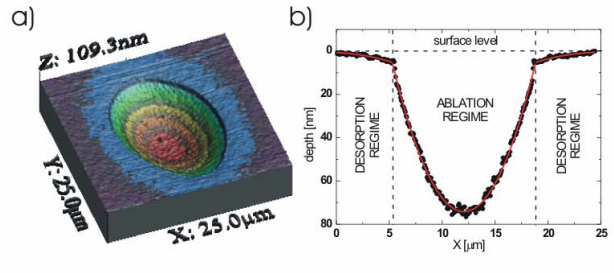

Fig. 1. (a) A crater created by the focused beam of FLASH at 21.7nm distinguishing between ablation and desorption regimes. (b) Transverse cross-section fitted by function (4) assuming a Gaussian beam profile.

As estimated from the fit, the maximum desorption efficiency η_D, i.e., the material removal efficiency at the sharp crater edge, is less than 10%, whereas the ablation efficiency η_A (saturated efficiency in the crater center) is close to 100%. Although the difference seems to be remarkable, the two efficiencies are significantly closer to each other for soft x-rays than they are for UV photons [25]. Accordingly, the desorbed depth exceeds half of a surface monolayer as it was defined by Haglund for UV radiation [20]. In conclusion, desorption is one order of magnitude more efficient for soft x-rays than for UV photons; therefore, Haglund's criterion should be modified for such energetic photons.

An additional ("intermediate") interaction regime has been revealed in PMMA. All three interaction regimes, i.e., ablation, intermediate, and desorption, are observable in Figs. 2(a) and 2(b) showing a shallow crater created by a single FLASH pulse of energy slightly above the ablation threshold. Under such irradiation conditions, the narrow intermediate region (see Fig. 3 below) gets spatially broadened and better distinguishable. In addition, the surface roughness, as can be seen in Figs. 2(b) and 2(c), varies with respect to a particular region of materials removal. Analyzing the AFM data by WSxM 4.0 Develop 12.3 software [26], we have determined that the intermediate region exhibits increased surface roughness and fulfills expectations of enhanced interaction instability in this regime. As shown in Fig. 2(c), the surface roughness is in the intermediate regime by factor of 4 and 2 higher than in the desorption and ablation regime, respectively. Explicit solution of integral formula (3) for efficiency curve introduced in Fig. 3 clearly indicates an existence of the intermediate region where both ablation and desorption processes may occur. Thus the response of the material should be in this region highly sensitive to local intensity fluctuations. The enhanced roughness observed in the intermediate area (Fig. 2(a) - I, Fig. 2(c) - red curve) is likely caused by that.

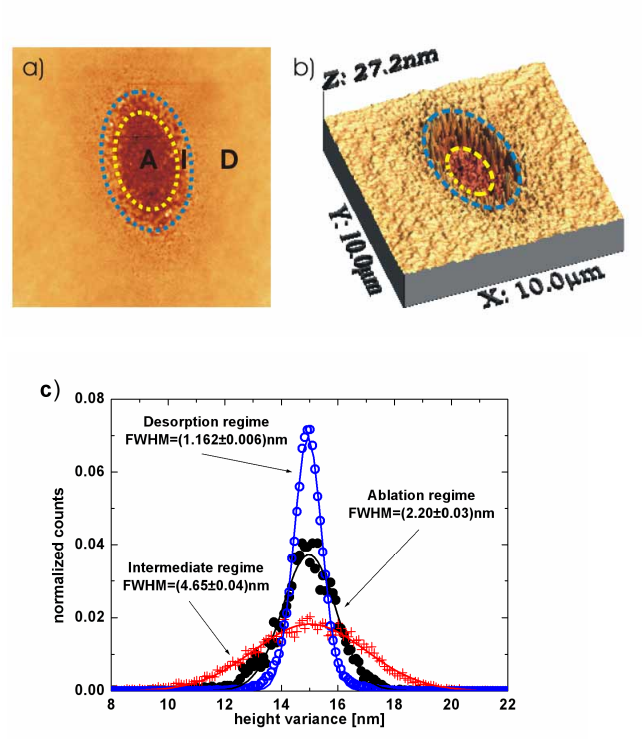

Fig. 2. (a) A shallow crater created by a pulse of radiation from FLASH at 21.7nm. The fluence is slightly above the threshold distinguishing the ablation, intermediate, and desorption regimes of material removal (A – the ablation region, I – the intermediate region, D – the desorption region). (b) AFM 3D morphology of the crater. (c) AFM surface roughness measurement for particular interaction regimes.

3. Interpretation

As it was proven recently due to absence of any thermal damage, surface imperfections, and bubbles [15-17], the PMMA ablation is governed mainly by a non-thermal process called bond scissions. Energetic photons break molecular chains and side groups releasing small molecular weight fragments which evaporate from irradiated surface into the vacuum. Subsequently, the lattice alteration and pulse energy losses lead to reduction of the efficiency of charge carrier thermalization and also the heat propagation into the pristine material suppressing the role of thermal damage to the sample (see [10]).

Let us assume that non-thermal photodecomposition is essentially more efficient, and thereby we neglect the role of the thermal decomposition (thermal ablation). In PMMA, which is a dielectric material exhibiting low radiation resistance, the absorbed energy is not efficiently thermalized and delocalized due to the heat conduction and charged carrier diffusion. Therefore, the local absorbed dose can be expressed as:

$$\varepsilon(x,y,z) = \varepsilon_0 f(x,y,z) e^{-z/l_{at}}, \qquad (1)$$

where ε_0 is a peak dose, f(x,y,z) is a beam profile function where the z-axis is perpendicular to the sample surface plane, x and y are in the plane of the sample, and l_{at} is the attenuation length at given wavelength coming from the Lambert-Beer absorption law. This expression is time-integrated; thus, assuming a Gaussian temporal pulse profile $\sim\exp(t^2/\tau^2)$, the relation between peak dose ε_0 and peak intensity I_0 is $\varepsilon_0 = \pi^{1/2}\tau I_0/l_{at}$. Further restrictions on the spatial profile f(x,y,z) function are needed. Considering slowly varying beams only, we ignore the z-dependence of the f and express it as f(x,y). In fact it means that the attenuation length and the

crater depth are much shorter than Rayleigh's parameter of the beam. Separation of transverse x,y and longitudal z parts in Eq. (1) greatly simplifies the following response calculations of the irradiated material.

Let us define the dose-dependent efficiency, $\eta(\varepsilon)$, of material removal for elemental solids as a ratio between number of atoms per unit volume removed by a single pulse, $n_R(\varepsilon)$, and number of atoms per unit volume contained in the pristine material, n:

$$\eta(\varepsilon) = \frac{n_R(\varepsilon)}{n}. \tag{2a}$$

For multi-elemental compound materials the total efficiency $\eta(\varepsilon)$ may be expressed as a weighted average in a following form:

$$\eta(\varepsilon) = \frac{\sum_i M_i n_R^i(\varepsilon)}{\sum_i M_i n_i}, \text{ where } \sum_i n_i = n \tag{2b}$$

Here i denotes a summation over particular elements, $n_R^i(\varepsilon)$ and n_i indicate removed and total particle densities of i-th element; $n_R^i(\varepsilon)$ must be strictly less than or equal to n_i. M_i represents a molar mass of i-th element, and n is a total particle density. It should be pointed out that atoms are considered here just to avoid a need of microscopic description of the particular species removed from the irradiated surface. The single-elemental efficiency definition (2a) is chosen to simplify further calculations in this paper.

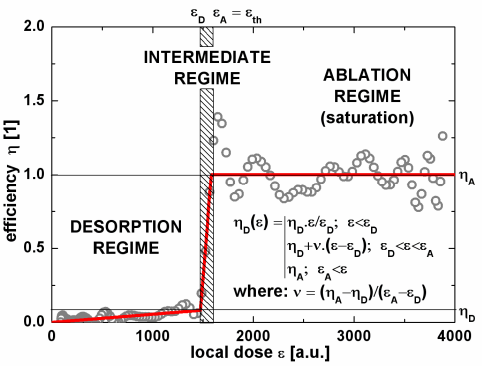

Fig. 3. Plot of the dependence of the material removal efficiency on the local dose (red solid line) fitted to the measured efficiency data (open circles).

The definition in the removal efficiency allows us to distinguish between desorption and ablation in dependence on the local dose. In Fig. 3 an approximate linearly interpolated plot of the material removal efficiency fitted to the measured efficiency data is shown introducing schematically three regimes of interaction. First, desorption occurs for the local dose below ε_D, where the material removal efficiency remains lower than η_D, defined as the maximum desorption efficiency. This means that a single photon is able to release a fragment (atom or molecular fraction) from and from beneath the material surface with some non-zero probability by breaking its bonds to the closest neighbouring atoms. This single-photon action was proposed and distinguished from the ablation, i.e., collective phenomenon, earlier [13,15,27], but not yet investigated quantitatively within one model taking into account both phenomena. Typically, the desorption regime is observed at tails of the beam where the absorbed dose is sufficiently low. Secondly, the intermediate regime is expected between local doses ε_D and ε_A, where the efficiency increases rapidly to the constant (saturated) value. In short, at this sharp rising edge, sufficient number of photons has broken all of the atomic

bonds making the central atom free. In addition, the steep gradient of the efficiency may be responsible for interaction instabilities (see Figs. 2(a)-2(c)) resulting in the local surface roughness increase. Finally, when the local dose exceeds ε_A, the efficiency saturates at value η_A (saturated ablation efficiency) and collective ablative photodecomposition occurs. Further continuation of the efficiency curve is complicated and could be affected by thermal effects.

The local dose dependent efficiency curve and the spatial distribution of the absorbed dose control the morphology of the desorbed/ablated imprint. The crater profile, i.e., the depth at position (x,y), satisfies following formula of local and sudden response induced by a single pulse:

$$d(x,y) = l_{at} \int_0^{\varepsilon_0 f(x,y)} \frac{\eta(t)}{t} \cdot dt \,, \tag{3}$$

where t is an integration variable. Feasibility of this integration depends on the behavior of $\eta(t)/t$ as t approaches zero. For the efficiency function introduced in Fig. 3, the integrability condition is clearly fulfilled. The importance of Eq. (3) is in its independence of a physical interaction model, originally encoded in the efficiency function $\eta(\varepsilon)$; therefore, it is applicable to any dose-dependent efficiency function satisfying the integrability condition.

Let us furthermore neglect the intermediate regime of interaction, i.e., study the limiting case $\varepsilon_A \rightarrow \varepsilon_D$ where ε_A is the ablation threshold dose ε_{th}. Under this condition, the single-shot crater shape can be described as follows:

$$d(x,y) = \begin{cases} l_{at}\eta_D \dfrac{\varepsilon_0}{\varepsilon_{th}} f(x,y); & \varepsilon_0 f(x,y) < \varepsilon_{th} \\ l_{at}\left(\eta_D + \eta_A \ln\left(\dfrac{\varepsilon_0}{\varepsilon_{th}} f(x,y)\right)\right); & otherwise. \end{cases} \tag{4}$$

The first formula in (4) represents the desorption regime where the depth morphology of the imprint is proportional to the intensity in transverse beam profile. Therefore, the desorbed crater corresponds to a direct footprint of the incident beam. The second formula describes ablation and, except for a small additional desorption term ($l_{at}\eta_D$) is consistent with observations reported in [22]. In other words, Eq. (4) extends the model reported in Ref. 22 below the ablation threshold.

Under certain ideal conditions, this model should be able to predict crater shape created by multi-shot irradiation. Keeping all of the beam parameters constant and assuming an ideal response of the material, the final profile d(x,y) can be expressed as a sum over all of particular single-shot imprints. In a real case, the calculation may be complicated due to beam instabilities, e.g., energy fluctuations, pointing jitter, and non-trivial time-evolving efficiency function $\eta(\varepsilon)$.

3. Multiple-shots damage experiments

The ablation threshold of PMMA at 32nm was recently found to be as low as ~2mJ/cm^2 [16,17,22]; therefore, to prove the below threshold process of laser induced desorption we have used a high-order harmonics (HOH) source at Laboratoire d'Optique Apliquée (LOA), Palaiseau/France. This source provides sufficiently low energy per a single pulse, excellent stability, and high repetition rate. A pulse energy less than 10pJ corresponds to a fluence of 0.3mJ/cm^2 (see Tab. 1) and lies well below the single shot ablation threshold. Therefore the beam-surface interaction may cause materials desorption only.

The amplified IR pumping Ti:Saphire beam (pulse energy E = 6mJ, pulse duration τ = 35fs, wavelength λ = 800nm) mixed with the HOH's beam was filtered out by a thin aluminium foil after exiting the argon-filled cell. The beam was then focused onto a sample using an off-axis Mo/Si multilayer parabolic mirror (OAP) with a focal length of 65mm. The

mirror coating was designed to exhibit maximum reflectivity for 25th harmonic order of Ti:Saphire (32nm). The angle between incident and reflected beams was 5°. A 500-nm layer of PMMA (Silson; UK) was mounted on a micrometric positioning stage and was irradiated at different distances from the focal plane for various exposure times, i.e., for various number of accumulated shots.

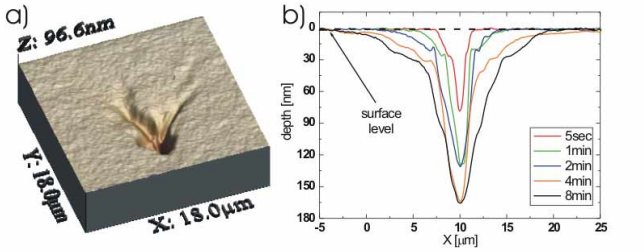

Fig. 4. (a) Desorption (photo-etched) imprint of tightly focused HOH's beam in PMMA induced by 5000 shots (5s exposure). (b) Transverse X cross-sections for various irradiation times.

An AFM image of the desorption imprint in PMMA induced by 5000 shots of tightly focused HOH radiation is shown in Fig. 4(a). In the main crater's vicinity, a broad coma aberration of the focusing mirror appears. However, the main crater diameter remains narrower than 1.5μm. Surprisingly, the maximal crater depth is not proportional to the number of accumulated shots and the etch rate decreases in time (see Fig. 4(b)). In fact this means that for longer irradiation times, i.e., for higher doses accumulated in PMMA, radiation resistance arises. The effect of etch rate deceleration most probably originates in PMMA radiation-chemical changes induced by HOH pulses. We suggest that the process of PMMA interchain cross-linking [15,28-32], competing with chain scissions, results in a reduction of desorption efficiency and an increase of ablation threshold.

Considering the removal efficiency evolving in time, we cannot use PMMA for long-time exposure beam profile measurements unless we understand the mechanisms of surface hardening occurring there; however, for short-time exposures the PMMA imprint follows more or less reliably the real beam profile.

4. Conclusions

Multiple-shot material desorption has been observed in PMMA using high-order harmonics at wavelength of 32nm. Effective material removal has been proved even very well below the single-shot ablation threshold. Varying the number of accumulated shots, a process of radiation-initiated surface hardening has been revealed. The morphology of short-time exposure imprints corresponds to the transverse beam profile. AFM investigation of crater shape may be used for direct beam imaging for low-peak-power soft x-ray sources such as high-order harmonics. Long-time exposures significantly alter the physical and chemical properties of the PMMA surface, making the beam profile reconstruction very difficult, if not impossible.

Single-shot below-threshold interaction was first observed in PMMA irradiated by focused FLASH pulses at 21.7nm. Single-shot desorption is significantly less efficient than ablation; therefore it is often overlapped by surface features caused by the ablation. However, sufficiently sensitive AFM measurements have enabled us to visualize and resolve desorption phenomena. The highly-resolved crater shape corresponds well to the prediction obtained by means of non-thermal desorption/ablation model introduced in this paper. We estimate the maximal desorption efficiency of PMMA to be below 10%, whereas saturated ablation efficiency reaches nearly 100%. Furthermore, an intermediate regime of interaction has been observed. High interaction instability being predicted by the absorption/desorption model has also been confirmed in the FLASH interaction experiments.

Acknowledgements
This work was partially funded by the Czech Ministry of Education from the National Research Centers program (Projects LC510 and LC528) and program INGO (Grant LA08024), Academy of Sciences of the Czech Republic (Grants Z10100523, IAA400100701, and KAN300100702), Czech Science Foundation (Grant 202/08/H057), State Committee for Scientific Research of the Republic of Poland (Grant No72/E-67/SPB/5.PR UE/DZ 27/2003-2005), Swedish Research Foundation and the European Commission (Grants FP6 NEST-Adventure n. 012843, TUIXS - Table-top Ultra Intense XUV Sources, FP7 INFRASTRUCTURES-2007-1 211737 HiPER - European High Power Laser Energy Research Facility, G1MA-CI-2002-4017, CEPHEUS, LOA001036, LASERLAB and RII3-CT-2004-506008, IA-SFS). A part of this work was performed under the auspices of the U.S. Department of Energy by Lawrence Livermore National Laboratory under Contract DE-AC52-07NA27344.